CDF/ANAL/TRACKING/CDFR/10938
Version 0.1
May 6, 2013

Measurement Analysis of Silicon Annealing at the CDF II Detector: DRAFT 1

K. J. Knoepfel and M. Stancari
Fermi National Accelerator Laboratory

Abstract

We present analysis results of the silicon annealing measurement made on the CDF II detector in October of 2011. The analysis motivation and methodology are presented, along with a description of the expected annealing behavior due to the Hamburg model. The operational aspects of the annealing measurement are not discussed in this document.

After the course of one month of annealing, the bias currents decreased by an average of $xx\%$, and the depletion voltage decreased an average of $yy\%$. A method for accounting for self-heating effects was developed and implemented in the bias current-vs-voltage fitting method. The evolution of the "knee voltage" was tracked over the course of the month.

The results of this study are to be included in a document to be submitted to Nuclear Instruments and Methods in Physics Research, Section A.

1 Introduction

Table 1: Ladders tested in annealing measurement.

	L00 Ladders		SVX Ladders					
Group 1	LB0W5L3	LB1W2L3	SB0W10L1	SB1W9L3	SB2W11L0	SB3W5L3	SB4W4L0	SB5W3L1
Group 2	LB0W0L3	LB1W3L3	SB0W3L3	SB1W1L0	SB2W0L1	SB3W8L3	SB4W7L0	SB5W6L1
Group 3	LB0W1L3	LB1W4L3	SB0W5L3	SB1W4L0	SB2W3L1	SB3W11L3	SB4W10L0	SB5W9L1
Group 4	LB0W2L3	LB1W5L3	SB0W8L3	SB1W11L0	SB2W6L1	SB3W0L0	SB4W2L1	SB5W1L3
Group 5	LB0W3L3	LB1W0L3	SB0W11L3	SB1W10L0	SB2W9L1	SB3W3L0	SB4W5L1	SB5W8L3
Group 6	LB0W0L1	LB1W3L1	SB0W0L0	SB1W2L1	SB2W1L3	SB3W6L0	SB4W9L1	SB5W7L3
Group 7	LB0W1L2	LB1W4L2	SB0W3L0	SB1W5L1	SB2W4L3	SB3W9L0	SB4W11L1	SB5W10L3
Group 8	LB0W2L0	LB1W5L0	SB0W5L0	SB1W8L1	SB2W7L3	SB3W1L1	SB4W0L3	SB5W2L0
Group 9	LB0W3L1	LB1W0L1	SB0W9L0	SB1W11L1	SB2W9L3	SB3W6L1	SB4W3L3	SB5W5L0
Group 10	LB0W4L2	LB1W1L2	SB0W1L1	SB1W0L3	SB2W2L0	SB3W7L1	SB4W6L3	SB5W8L0
Group 11	LB0W5L0	LB1W2L0	SB0W4L1	SB1W3L3	SB2W6L0	SB3W10L1	SB4W9L3	SB5W11L0
Group 12	LB0W4L3	LB1W1L3	SB0W7L1	SB1W6L3	SB2W8L0	SB3W2L3	SB4W1L0	SB5W0L1

2 Useful Reminders and Necessary Definitions

The definitions below will be helpful in understanding the scope of this paper.

E_{gap} or E_g	Gap energy of silicon (about 1.2 eV)
Ladder	Fundamental module in CDF silicon detector; comprised of three silicon sensors
I_{bias}	Bias current of each ladder
V_{bias}	Bias voltage of each ladder
V_{op}	V_{bias} of each ladder during data-taking operation
V_{dep}	Depletion voltage of each ladder
$\widetilde{V}_{\text{dep}}$	V_{dep} of each ladder, as determined by V_{knee}-to-V_{dep} mapping
V_{knee}	Knee voltage of each ladder, defined in Sec. 4.1

2.1 Determination of V_{dep}

Theoretically speaking, the depletion voltage V_{dep} is the value of V_{bias} required to fully deplete the active detector region of any charge carriers. The formal definition is

$$V_{\text{dep}} \approx \frac{q_0}{2\epsilon\epsilon_0}|N_{\text{eff}}|d^2 \tag{1}$$

where q_0 is the charge of the electron, $\epsilon\epsilon_0$ is the permittivity of silicon, N_{eff} is the effective doping concentration, and d is the total width of the p-n junction. In the context of test beam setups, the value of V_{dep} is determined by measuring the capacitance of the sensor as a function of V_{bias}. The CV curve exhibits a kink at high voltage, and the intersection of two lines that describe the data before and after the kink unambiguously defines V_{dep}.

For an operating experiment, the capacitance cannot be measured practically, so V_{dep} must be measured using an alternate way. The procedure for how this is measured at CDF is mentioned in some detail in CDF Note 10XYZ. To briefly summarize, we define V_{dep} as the voltage that maximizes the signal collection in a given data-collection time window. The number of hits on a silicon ladder from minimum-ionizing particles is collected as a function of V_{bias}. For a given V_{bias} setting, this distribution closely follows that of a Landau distribution, convoluted with a Gaussian, which accounts for experimental resolution effects. The location of the peak of the Landau distribution is mapped against the corresponding V_{bias} value. The overall shape of the mapping looks like a sigmoid distribution (especially for the ϕ-side ladders). After fitting to a sigmoid, the depletion voltage is defined as the location where the fit exceeds 95% of its asymptotic value as $V_{\text{bias}} \to \infty$. This definition of V_{dep} is assumed throughout this document.

For the annealing study presented here a signal source (i.e. source of MIPs) were not available, and so V_{dep} needed to be determined in other ways and using other metrics (Sec. 6 and 4.1).

3 Analysis Complications and Their Resolutions

In addition to the many complications that arose in performing the measurement (not discussed in this document), there are several analysis complications that arose.

3.1 Missing Data Entries in ntuples

To construct IV curves, we need to reverse bias the ladders for various voltage settings. We allow each ladder to remain biased for either 3, 6, or 21 minutes, depending on the voltage setting. Three minutes are chosen for the lower voltages, of which it was necessary to accurately characterize the turn-on of the IV curve. Six minutes is chosen for the higher voltages, and twenty-one minutes is used for the last voltage point to ensure stable current and voltage measurements.

For each voltage setting, 36, 72, or 252 updates are possible to the ntuple whether the voltage setting lasted for 3, 6, or 21 minutes, respectively. However, updates are only written to the ntuple if one of the monitored quantities of the ladder group associated with the crate changed within a 5-second window. Consequently, if the quantities were stable throughout a five-second period, the ntuples were not updated, and gaps in time would exist between data updates. As we are interested in unique values for the current I_{bias} and voltage V_{bias} for a given voltage setting, an average of the IV measurements for a given voltage setting must be performed (Sec. 3.2). This average will be biased, however, if the ntuple of an overly stable ladder does not record the IV measurements for times when the crate was stable. To fix this issue, we *insert* the missing IV measurements if the time elapsed between two consecutive updates is greater than 5 seconds.

3.2 Unique IV Values for Voltage Setting

As there are 36, 72, or 252 IV measurements per voltage setting, a unique IV value must be assigned for each setting. Figure 1 shows the plotted current I_{bias} *vs.* the time of the scan, measured relative to the beginning of the day. As can be seen, for the beginning of each voltage setting, there is a thermal "turn-on" for each current reading, due to the inability of any system to respond instantaneously to a change in operating parameters. This "turn-on" region should thus be avoided in the averaging procedure. The chosen method thus includes points $n-5$ to $n-1$ for a voltage setting with n points measured. This gives enough time for the ladder to stabilize, and avoids using the last point which sometimes is recorded too close to a voltage change and can thus throw off the average. These averages (current shown in Fig. 1) are used in the IV fit procedure (Sec. 4), where half of the spread in the IV measurements used in the voltage-setting average is assigned as the uncertainty in the IV average.

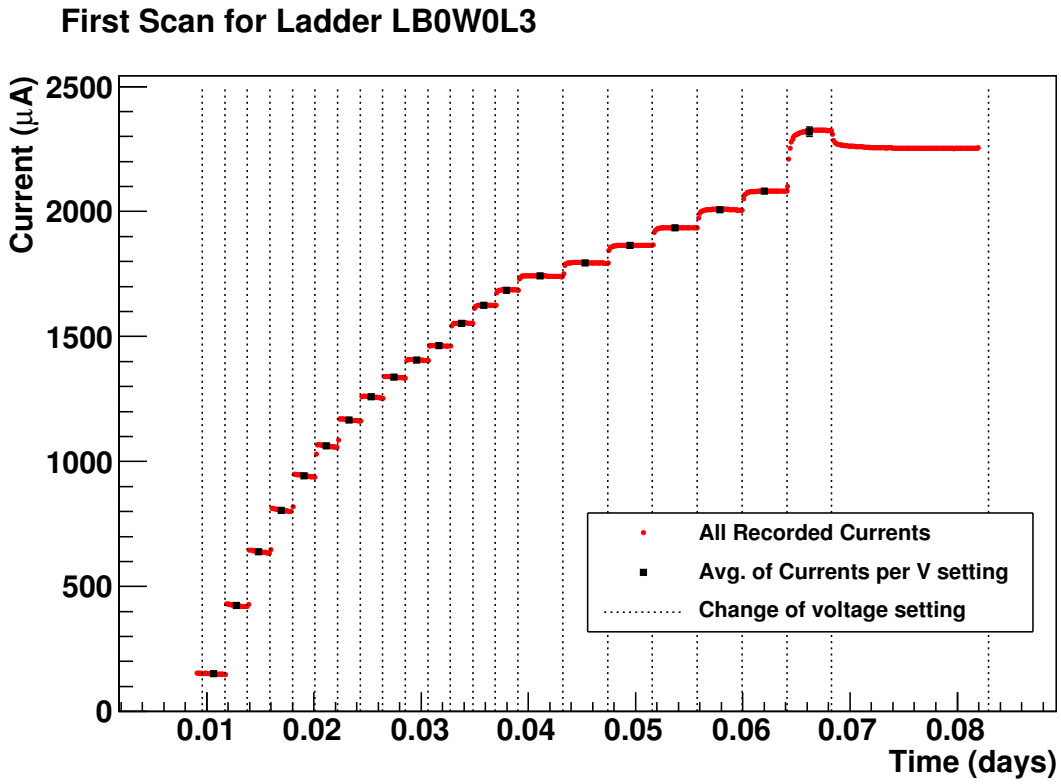

Figure 1: Current *vs.* time for the first scan of ladder LB0W0L3. The average for the last voltage setting is not present as that setting is used primarily for assessing changes in current, and not tracking V_{knee} changes. The offset in the horizonal axis is chosen for illustrative purposes. Similar plots can be made for the voltage.

4 Current-Voltage Fit Procedure

As mentioned previously, no signal source is used in the annealing procedure, but rather the shape of the IV curve is used to infer the depletion voltage V_{dep}. Although such an inference is possible in practice, the uncertainty in the various fit parameters make determining V_{dep} impracticable. Instead, we fit the IV curve to an empirical function and determine the "knee" location of the voltage—i.e. the voltage at which the IV curve turns over.

4.1 Fit Function and the Knee Voltage

A description of the IV dependence of a p-n junction is given in App. A. As discussed therein, we choose an empirical function to fit the IV pairs we measure for a given voltage setting:

$$I_{\text{bias}}(V_{\text{bias}}; \mathbf{p}) = p_0 - p_1 \exp\left(-p_2 V_{\text{bias}}^{p_3}\right) + p_4 V_{\text{bias}} \ , \tag{2}$$

where the p_i represent parameters to be fitted. The kneee voltage V_{knee} is extracted by locating the voltage where the slope of the fitted IV curve reaches 5% of its maximum value, relative to the difference of the maximum and minimum slopes. In mathematical form:

$$V_{\text{knee}} = \arg\left[\frac{\partial I}{\partial V} \;\middle|\; \frac{\partial I}{\partial V} = 0.05 \times \left(\max \frac{\partial I}{\partial V} - \min \frac{\partial I}{\partial V}\right)\right] \ .$$

The uncertainty in V_{knee} is determined by drawing 10 000 random variates from the set of fit parameters (assumed to be Gaussian-distributed about their uncertainties), using the full correlation between them as determined by the MINUIT fit, and then extracting V_{knee} from each function as specified by each random draw. The uncertainty is assigned as the rms of the distribution of V_{knee} values from the 10 000 draws.

4.2 Fit Specifics

Fit Range. For each fit, the lowest-voltage point is omitted as is a certain percentage of the upper voltage range. The default fit range includes voltage points up to 80% of the maximum bias voltage V_{bias}. If the fit does not converge, the range extends to 90%. Finally, if that fit does not converge the entire fit range (modulo the first low-voltage point) is used. The motivation for this method is that self-heating effects begin to appear at higher voltages, thus affecting the determination of V_{knee}. Although this is not a problem in itself, we prefer to utilize a metric that is insensitive to self-heating effects, which only appear at higher temperatures, and not so much at the lower ones (as was the case during the nominal running conditions). Using the self-heating corrections as described in Sec. 7.1 significantly reduces any dependence on this effect; but to avoid sensitivity to any residual self-heating effects, we restrict the nominal fit range to 80%.

Self-heating corrections for warm scans. For L00, self-heating effects on the IV curve become non-negligible at high enough temperature and voltage. It is therefore important to account for these effects when fitting the observed IV points; not doing so can potentially lead to a biased determination of the knee voltage V_{knee}. The handling of these corrections is described in Sec. 7.1.

Uncertainties used in fits. As mentioned in Sec. 3, an averaging procedure was utilized to obtain a reliable measurement of the bias current I_{bias} and operating voltage V_{op} for a given voltage setting. One half of the spread of bias-current values for a given voltage setting is used as an uncertainty in the fit procedure. An additional uncertainty of 1 μA, corresponding to the uncertainty of the least-significant bit, is added in quadrature to this spread. Since the self-heating temperature correction is correlated for the entire scan, we do *not* introduce its uncertainty in the fitting procedure. Rather, we fit multiple times to the central, and ± 1 standard deviation correction values, and then we take the resulting spread of the knee voltage and add

it in quadrature to the error-propagation uncertainty (described above) for a given knee-voltage determination. See Sec. 7.2 for more details.

4.2.1 Example: Scan 27 of LB0W0L3

To illustrate the above features of each fit, we provide an example from ladder LB0W0L3. Figure 2 shows the original uncorrected, but averaged data points in black, and the temperature-corrected points in blue. The IV fit is performed on the temperature-corrected IV points, using the central temperature correction and the parameterization of Eq. (2). The bottom plot shows the data-fit subtraction, illustrating good agreement in the chosen fit range. Also shown is the extracted knee voltage, and its associated uncertainty. The associated pulls for each of the fit parameters are shown in Fig. 3, illustrating the robust behavior of the error-propagation study. The means of the pull distributions are consistent with zero at better than the 1% level (exp. statistical uncertainty 1%). The widths of the pull distributions are all consistent with unity, as expected.

The V_{knee} distribution is shown in Fig. 4 for the 10 000 random draws from the MINUIT-returned fit result. The central value is taken as the fitted value from the IV data points. Despite the asymmetric distribution shown in Fig. 4, the V_{knee} uncertainties are set equal to the rms value of the distribution, and assumed to be symmetric.

Value of χ^2/ndf. As seen in Fig. 2, the χ^2/ndf is not very consistent with one, as would be desirable if the fit function well describes the underlying distribution of the data you are fitting. As one can see in the "Δ Current" portion of the figure, most of the contributions to the χ^2/ndf come from the low-voltage portions of the graph, where it is very difficult to describe the thermal turn-on. This "undulating" feature of the residuals plot is common to each fit, and is therefore a correlated mistake across the entire analysis. Since much of our analysis requires *comparison* of these fits, we believe this systematic effect largely cancels, or is at least small compared to other uncertainties we take into account. In addition, the fit appears to describe well the data above the turn-on region, making the V_{knee} determinations largely insensitive to this low-voltage region.

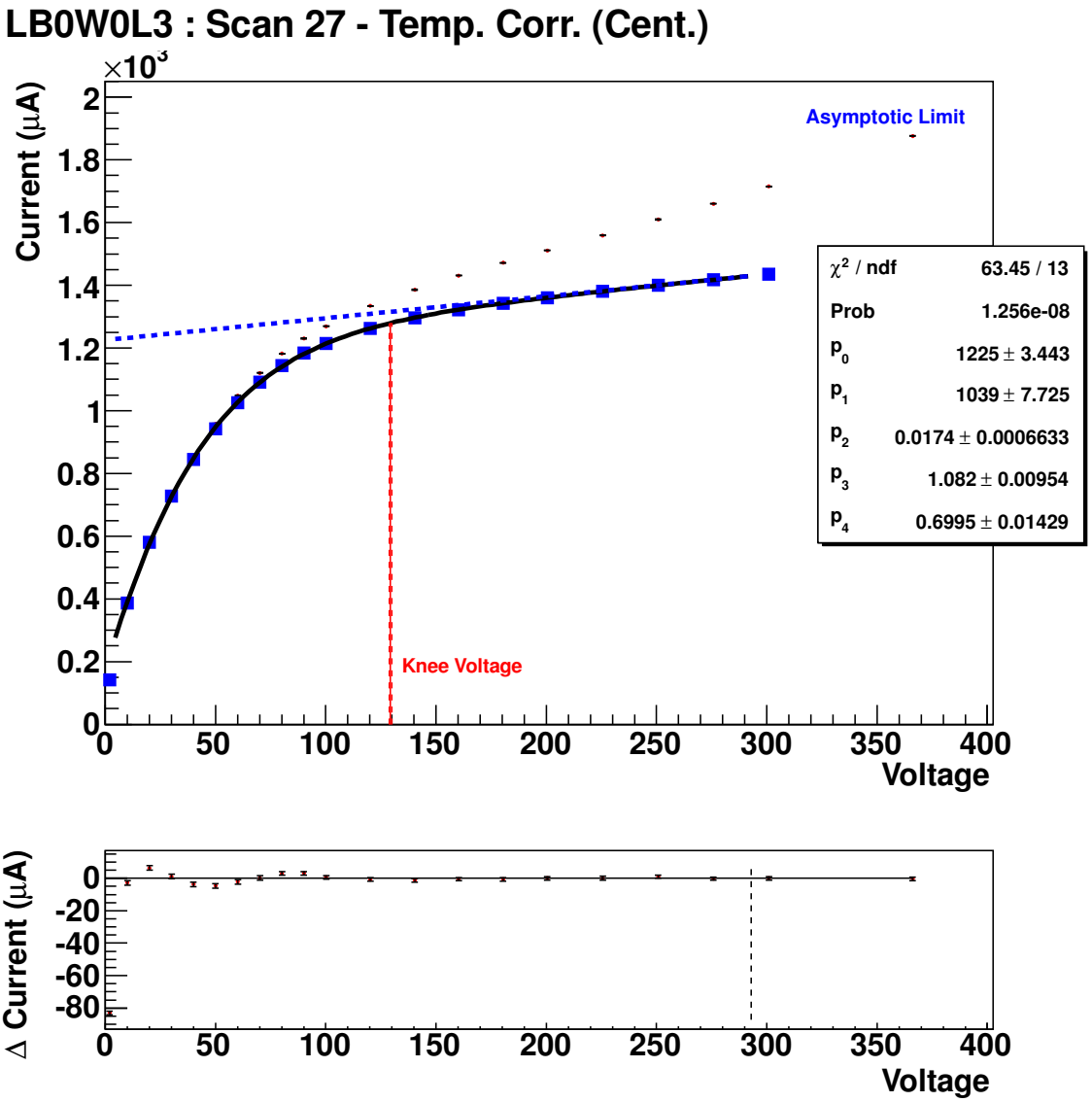

Figure 2: *IV* fit of warm scan 27, corrected for self-heating effects. Also shown are the uncorrected data points in black. The bottom plot shows the data-fit subtraction.

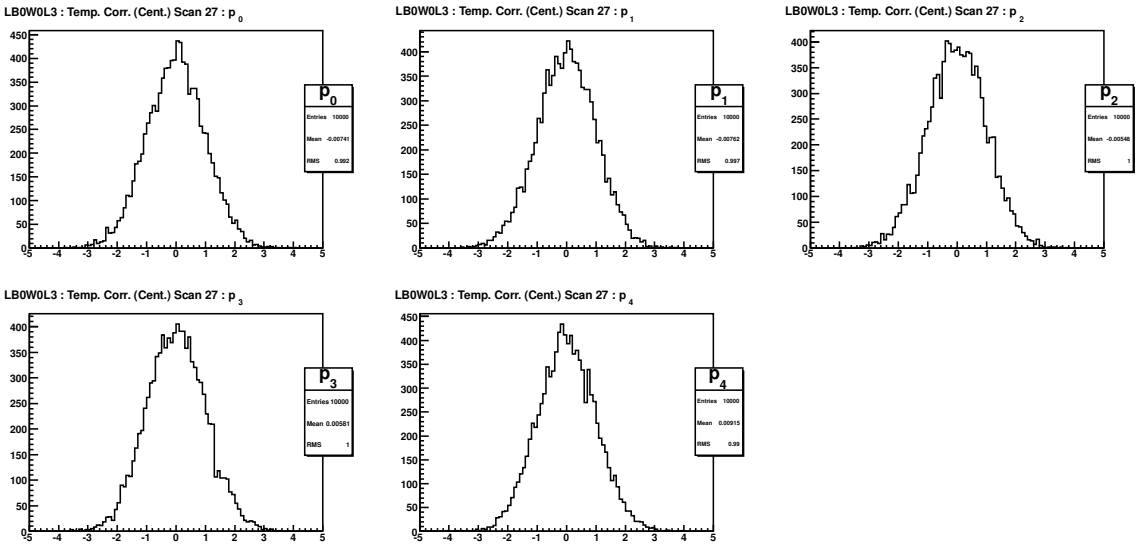

Figure 3: Pulls for the five parameters of the IV fit of temperature-corrected scan 27.

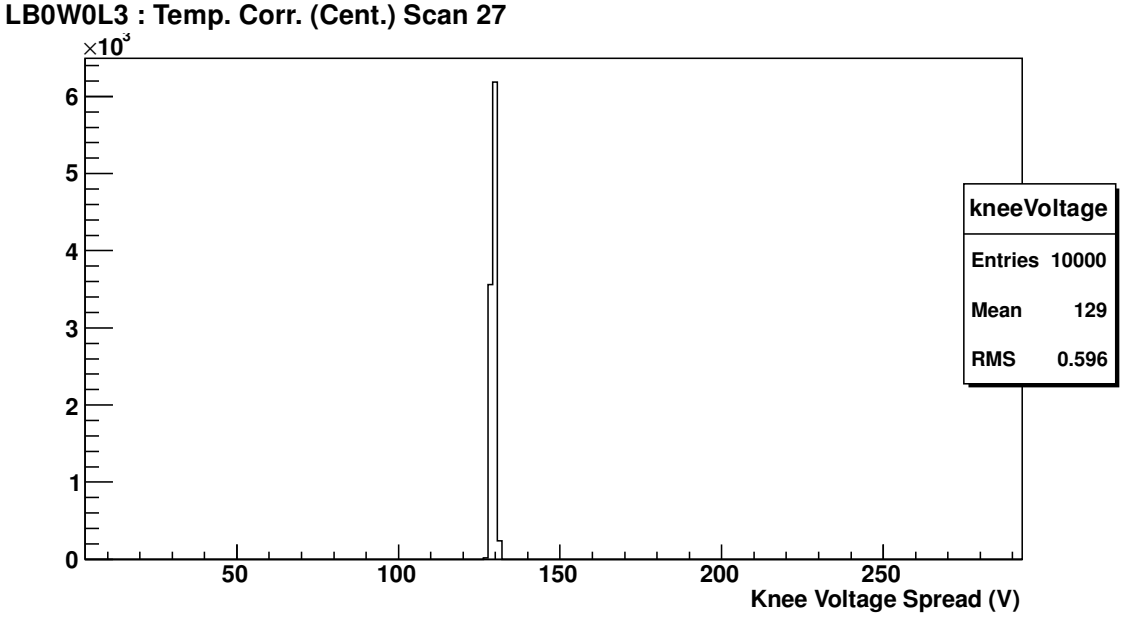

Figure 4: Distribution of V_{knee} results, based on 10 000 random draws from the MINUIT-returned fit result, where the fitted parameters of the IV curve are varied about their central values. Gaussian uncertainties on the fit parameters are assumed.

5 Change in Bias Current

The Hamburg model predicts the behavior of the leakage current of a sensor in the ideal condition that the sensor was irradiated during time A where no annealing happened, the temperature instantaneously changed to the *warm* annealing value, and then the sensor annealed during time B where there was no irradiation. The leakage current of an ideal sensor at a given temperature after time A and before time B is directly proportial to the fluence the sensor was exposed to. We will call this I_0. During time B, the current decreases from its maximum value I_0. The Hamburg model parameterizes this decrease with the sum of five exponentials and a constant. The Hamburg model incorporates the temperature dependence of the current decrease by scaling the time axis with a temperature correction factor. (Mathematical formula for both is in Moll's thesis near p 100, will be part of an earlier section of the NIM article.) At room temperature the time constants of the five exponentials are 18 minutes, 119 minutes, 0.76 days, 10.28 days and 61.94 days. The time constants are in principle larger for 18 deg C, but Moll's thesis does not quantify the temperature scaling. We expect our measurements to be sensitive to only one of the exponential terms in the sum, the one with a temperature-scaled time constant of 10.28 days. The remaining four exponential terms can be lumped together with the constant term.

Specifically, we have two measurements that can be compared with the Hamburg model for the current annealing: the *cold* and *warm* measurements. Before and after the annealing period, the currents were measured in cold conditions. The change in current can be compared with the Hamburg model prediction. This measurement is somewhat sensitive to any constant offset in the absolute value of the currents due to sensor defects or power supply miscalibrations.

The warm currents were measured at the end of each IV scan, roughly every 21 hours. This gives more information about the shape of the current decrease, and thus the time constant of the relevant exponential, than the cold result. However, the currents are significantly higher at the warm temperatures and the dissipative heating of the sensor is sufficient to raise its temperature during the measurement. The measured currents must be corrected back to the annealing temperature of 18 degC, and this correction is robust only for the narrow ladders of L00.

5.1 Cold currents

We can compare the measured currents under operating conditions before and after annealing and compare with the Hamburg model expectation. This has less information than the daily measurements, but there is no dissapative heating of the ladders to correct for.

I obtained the before currents from the time period $3924.0 < DSdays < 3294.3$ directly from the current plotter ntuples, taking the raw average of the entries in that window. It should be the time weighted average, but during running things were very very stable.

The after currents come from the special *operating currents* measurement at the end of the annealing period. There was roughly 25 minutes of thermal stability, and the time-weighted average was used for values in the range $3955.65 < DSdays < 3955.69$.

Figure does-not-exist-yet shows the ratio of after/before as a function of distance from the beam axis. This ratio is independent of ladder temperature in principle. The average is taken over all functional ladders in the layer. Suspected pinholes with noisy behaviour and abnormally high currents were excluded. Also shown on this figure is the expected value of the ratio from the Hamburg model, assuming the radiation doses of 12 fb-1, and no annealing whatsoever during the run. The error bars on the predictions reflect the uncertainty on the luminosity to radiation dose conversion.

Conclusions from figure here.

5.2 Warm currents

Figures 5 and 6 show the data for a typical narrow and wide ladder respectively. The red squares are the measured currents at full voltage as a function of annealing time. The currents at full voltage are determined by taking the average of the last five current readings and the uncertainty on this current is the rms of those readings or 5 μA, whichever is larger. This average value of the current is closer to the thermally stable value than the average obtained with the method described in section zz. The difference between this value and the thermally stable value is a systematic error common to all points for the same ladder at the same voltage, and its impact on the time constant extracted from the exponential fit is negligible. The blue circles are the equivalent current at 18 deg C, using the method described in section xx and appendix yy. A 3 parameter fit is performed (constant plus decaying exponential). The corrected current values are then recalculated with kappa+sigma (kappa-sigma), and these values fit to the same function. This shift in the fit parameter that results from the shift in kappa is quoted as a systematic error and plotted as a yellow error band.

Figure 7 displays the fitted time constant for each narrow ladder, and the combined result with a shaded band. The individual results are consistent with a single time constant, suggesting that potential differences among the ladders, due to temperature or radiation dose variations for example, are small.

5.3 Discarding the warm current analysis for the wide ladders

The average time constant measured for the wide ladders, about 22 days, is larger than the 18 days measured for the narrow ladders, and could be the result of a too-large temperature correct. The systematic error for κ for the wide ladders is $\sim$2 days compared with $\sim$0.5 days for the narrows. Combined with other inconsistencies in the data for the wide ladders, we conclude that the cost of pursing these data is much larger than the potential gain. In the NIM article, we will report results for the narrow ladders only for this analysis of the warm currents.

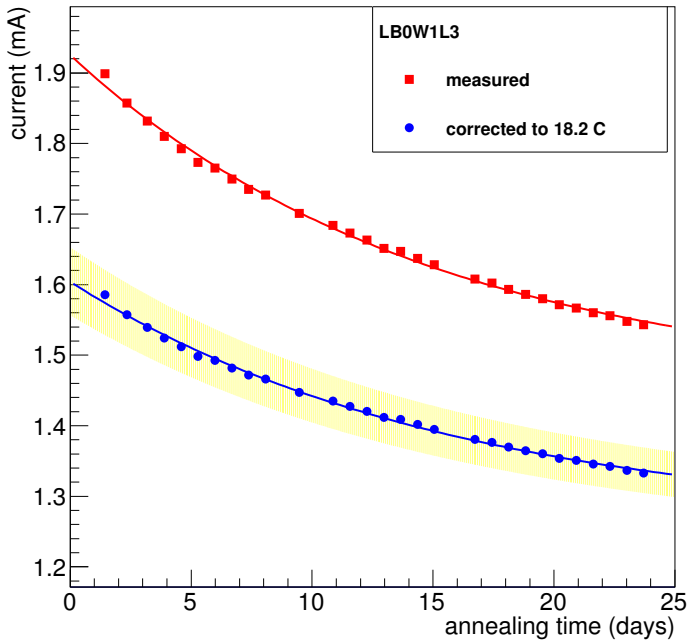

Figure 5: The time constant of this fit is $15.67 \pm 1.02 \pm^{0.16}_{0.15}$. The first error is statistical and the second systematic, derived from from the uncertaintly on κ.

5.4 SVX ladders

The decrease in current for the SVX ladders is *sim*5% or less before correcting for self heating. The power dissapation for these ladders is about 25% that for the narrows, so the temperature corrections are small perhaps negligible. The change in warm currents for three typical ladders is shown in fig **??**. The dancing of the layer 0 ladder is an artifact of the IVDataExtractor code, the time windows associated with each ladder group or both. The files for the individual scans appear to be truncated, and some or all of the data for the last voltage point is missing. This was understood by looking at the raw data from the current plotter ntuples and comparing with the numbers in the *Avg2* files. When only the early portion of the last voltage point is kept, the final number depends on how much data is missing, because the thermalization is not yet finished. This cutoff varies scan to scan, and thus causes the final current to fluctuate as observed in the plot.

Someone will have to fix this if we want to put the plot into the paper. But, the message is that these currents changed very little, when a xx% change was expected had they not annealed during the run.

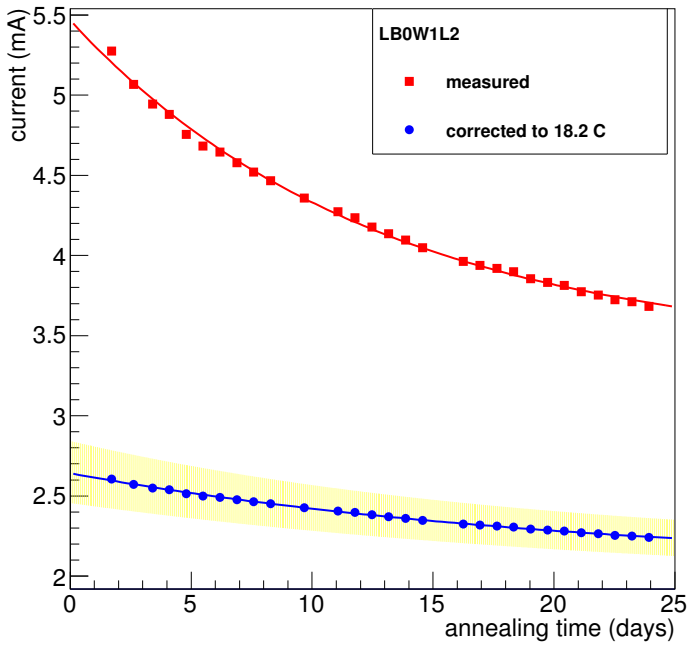

Figure 6: The time constant of this fit is $21.17 \pm 0.80 \pm^{3.46}_{2.19}$. The first error is statistical and the second systematic, derived from from the uncertaintly on κ.

6 Overall Change in Depletion Voltage

As the shape of the *IV* curve is the only feature we have to infer the depletion voltage, a reliable mapping from the V_{knee} to V_{dep} must be developed. As the behavior of each ladder is not guaranteed to be the same, we construct an individual map for each ladder.

6.1 Knee Voltage—Depletion Voltage Mapping

Two assumptions are made in constructing a V_{knee}-V_{dep} map:

1. a reliable metric of the *IV* curves can be obtained that uniquely associates the *IV* curve to a given value of the depletion voltage V_{dep}, and

2. as a mapping can only be made of pre-annealed data, we assume that the behavior of the metric before annealing corresponds to the behavior observed afterward.

To construct such a map, we take the *IV* curves measured during the L00 bias scans, which were made during nominal running conditions to determine the V_{bias} settings that would fully deplete the silicon ladders. We fit the bias-scan curves using the same functional form as shown in Eq. (2). We take the extract V_{knee} values and plot them against the measured V_{dep} values as obtained during the bias scan.

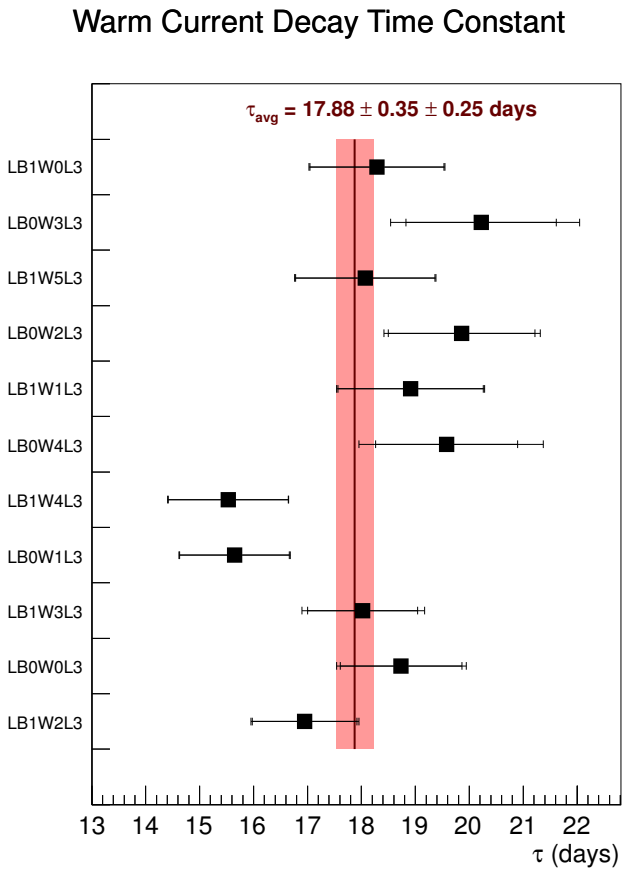

Figure 7: The best fit time constant for each narrow ladder. The inner error bars reflect the statistical uncertainty and the complete error bars the total uncertainty which includes the uncertainty on κ.

We use bias scans that were made for the following integrated luminosities of *recorded* data: 3.341, 4.042, 4.530, 5.253, 6.097, 6.544, 6.888, 7.025, 7.407, 7.761, 8.320, 9.009, 9.525, 10.369, and 10.626 fb^{-1}. Although V_{dep} measurements are, in principle, possible from each of these 15 luminosity points, typically only the V_{dep} measurements from six or seven luminosity points give usable information. Whereas the V_{knee} determination of each bias scan is usually reliable, the fit for determining V_{dep} often does not converge. This is a result of increased radiation damage on the silicon ladder as a functions of integrated luminosity.[1] As a result, many of V_{knee}-V_{dep} mappings only have a few points that are included in the linear fit. The paucity of points, however, is reflected in the uncertainty of the fit parameters, which are then propagated into all expressions used in determining the change of V_{dep} due to annealing.

In principle the observed relation between V_{knee} and V_{dep} can be used to suggest a functional form that maps between the two quantities. However, due to the often large

[1] A detailed study of this is given in CDF Note 10XYZ.

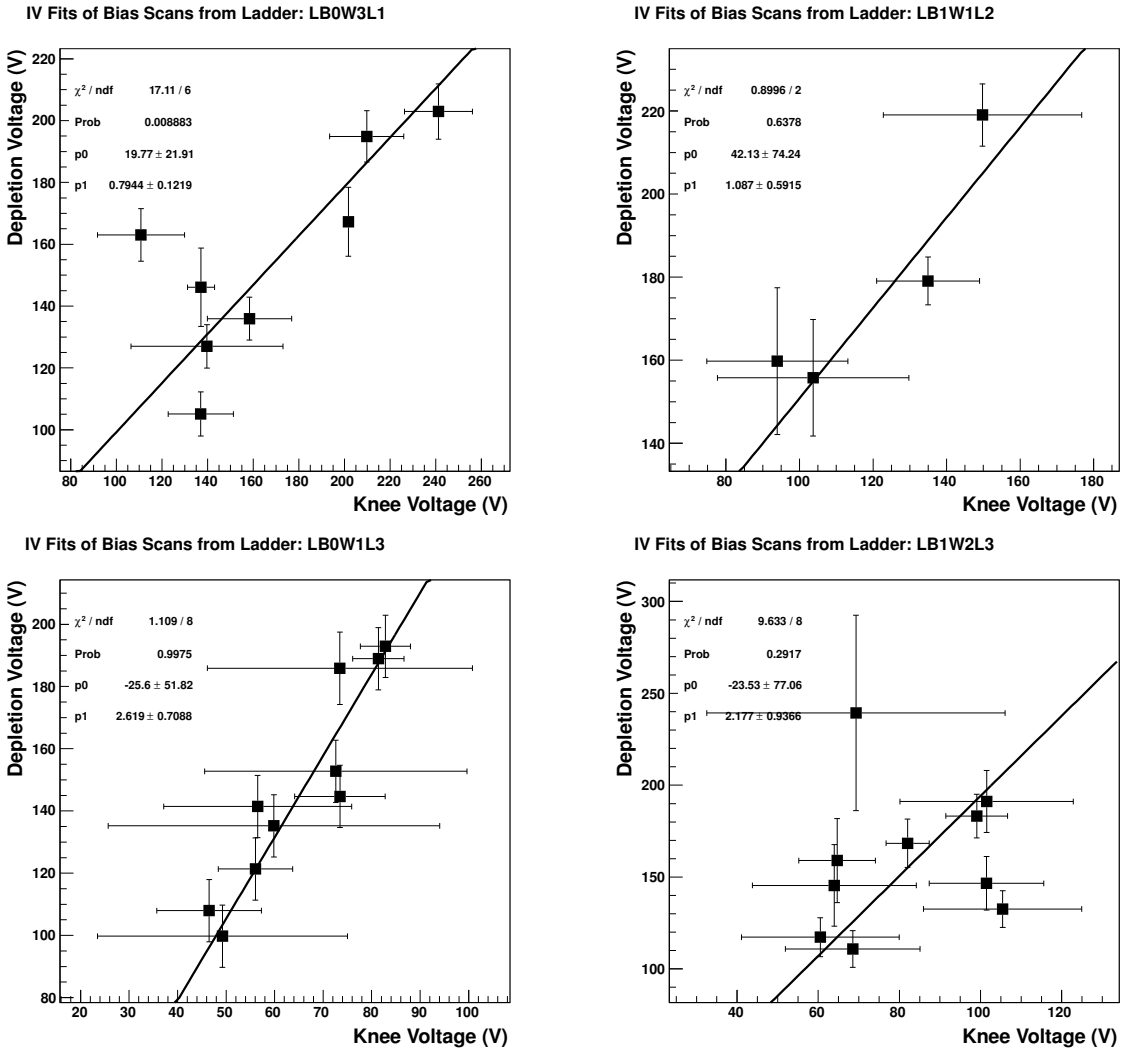

Figure 8: $V_{\rm knee}$-$V_{\rm dep}$ mappings for various L00 ladders. The uncertainties in both directions are taken into account using the "effective variance" fit method, as provided by ROOT.

uncertainties on the $V_{\rm dep}$ determinations, and the sometimes few points available for fitting (see previous paragraph), we are forced to assume a functional form. We choose a linear form $V_{\rm dep} = p_0 + p_1 V_{\rm knee}$, which is the simplest parameterization that uniquely associates a given value of $V_{\rm knee}$ to $V_{\rm dep}$.

Some sample mappings are given in Fig. 8. In general, the χ^2/ndf is very consistent with unity. The upper left plot gives the worst-case example. The ndf is determined by the number of fitted points minus the number of parameters in the functional form (two).

Using the mapping as described above, we can take the measured $V_{\rm knee}$ values from *cold* scans before and after annealing and associate them with a mapped depletion voltages $\widetilde{V}_{\rm dep}$. Note that it is imperative that this study be performed on scans that were made when the temperature conditions were the same as those during actual running as there is a non-trivial temperature dependence on $V_{\rm knee}$. We are therefore unable to use the mappings derived here to relate the warm-scan $V_{\rm knee}$ determinations to a physically meaningful $\widetilde{V}_{\rm dep}$ values.

We performed *IV* scans before and after annealing, where the conditions were set to those that would have been used during nominal running. We are interested in the decrease in the depletion voltage $\widetilde{V}_{\rm dep}$, which can be parameterized in terms of the absolute decrease $\Delta\widetilde{V}_{\rm dep} = \widetilde{V}_{\rm dep} - \widetilde{V}^0_{\rm dep}$ (given in units of V), and the relative change $\widetilde{V}_{\rm dep}/\widetilde{V}^0_{\rm dep}$, where $\widetilde{V}^0_{\rm dep}$ corresponds to the mapped depletion voltage before annealing. The uncertainties in both of these quantities is given below:

$$\begin{aligned}
\sigma^2\left(\Delta\widetilde{V}_{\rm dep}\right) &= \sigma^2(p_1)\left(V^0_{\rm knee} - V_{\rm knee}\right)^2 + p_1^2\left[\sigma^2(V^0_{\rm knee}) + \sigma^2(V^0_{\rm knee})\right] \\
\sigma^2\left(\frac{\widetilde{V}_{\rm dep}}{\widetilde{V}^0_{\rm dep}}\right) &= \left(\frac{\widetilde{V}_{\rm dep}}{\widetilde{V}^0_{\rm dep}}\right)^2 \Bigg[\sigma^2(p_1)\left(\frac{V_{\rm knee}}{\widetilde{V}_{\rm dep}} - \frac{V^0_{\rm knee}}{\widetilde{V}^0_{\rm dep}}\right)^2 \\
&\quad +2\rho\sigma(p_0)\sigma(p_1)\left(\frac{V_{\rm knee}}{\widetilde{V}_{\rm dep}} + \frac{V^0_{\rm knee}}{\widetilde{V}^0_{\rm dep}}\right)\left(\frac{1}{\widetilde{V}_{\rm dep}} - \frac{1}{\widetilde{V}^0_{\rm dep}}\right) \\
&\quad +\sigma^2(p_0)\left(\frac{1}{\widetilde{V}_{\rm dep}} - \frac{1}{\widetilde{V}^0_{\rm dep}}\right)^2 + p_1^2\left(\frac{\sigma^2(V_{\rm knee})}{\widetilde{V}^2_{\rm dep}} - \frac{\sigma^2(V^0_{\rm knee})}{(\widetilde{V}^0_{\rm dep})^2}\right)\Bigg]
\end{aligned}$$

where $\sigma(p_i)$ represents the standard deviation on parameter i, and ρ represents the correlation coefficient between p_0 and p_1. An implicit assumption is made that each measurement of $V_{\rm knee}$ is independent, and the uncertainties on the $V_{\rm knee}$ measurements are uncorrelated with those of p_0 and p_1.

As the mapped depletion voltage values are not necessarily expected to be of similar magnitude for all L00 ladders, it is more meaningful to use the relative change in mapped depletion voltages as the metric to be quoted. We do, however, quote both quantities (when possible) for each ladder. Table 2 change shows how the individual L00 ladders changed, both in terms of $V_{\rm knee}$ and in terms of $\widetilde{V}_{\rm dep}$. As the fits to the wide ladders were not stable (as evidenced by the shaded regions in the table), we consider only the narrow ladders in what follows.

We can combine the results from the narrow ladders to determine an average reduction in $\widetilde{V}_{\rm dep}$. A weighted average is taken of the eleven narrow ladders and plotted on Fig. 9; the uncertainties of each $\widetilde{V}_{\rm dep}$ determination are assumed to be uncorrelated. The average relative change in $\widetilde{V}_{\rm dep}$ is thus 0.73 ± 0.03, indicating an average reduction of roughly 25% in $V_{\rm dep}$ due to annealing over the course of one month.

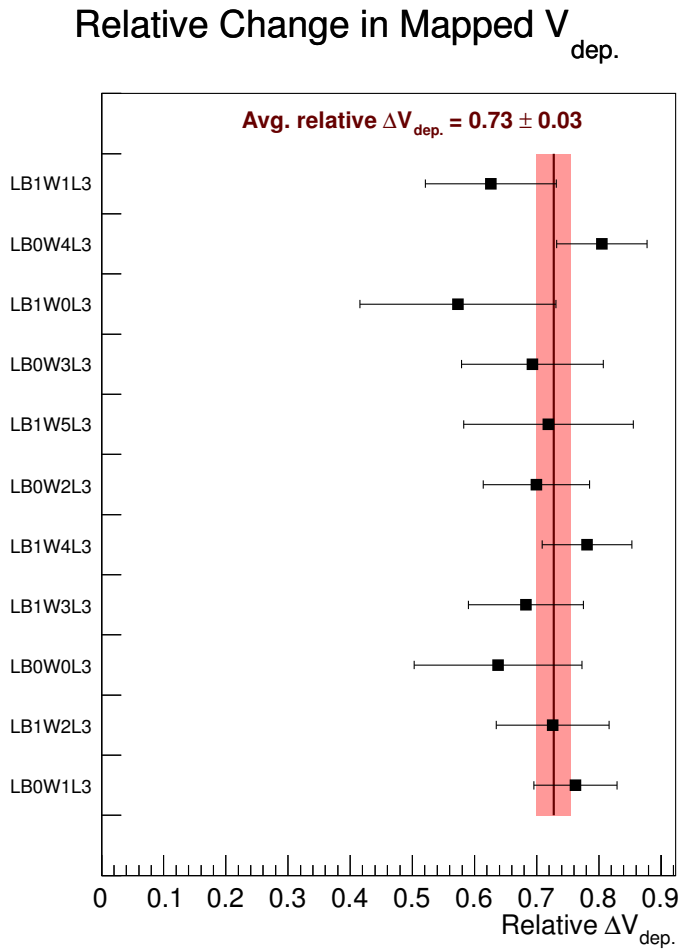

Figure 9: $\widetilde{V}_{\rm dep}/\widetilde{V}^0_{\rm dep}$ determinations for the eleven narrow L00 ladders, along with the weighted average.

Although it would have been desirable to track the evolution of $\widetilde{V}_{\rm dep}$ over the course of the full month of annealing, this was not practical as it would have required lowering the temperature from that of annealing to that of operating conditions for each IV scan taken. To track the evolution of the intrinsic depletion voltage of the ladder during annealing, we use the knee voltage, assuming it to be a meaningful metric of the behavior of the silicon. This study is discussed in Sec. 7.

Table 2: Changes in knee voltage V_{knee} and mapped depletion voltage $\widetilde{V}_{\text{dep}}$ for twenty-three L00 ladders. Shaded entries correspond to ladders where one or more of the *IV* fits failed.

Ladder	V^0_{knee} (V)	V_{knee} (V)	ΔV_{knee} (V)	$\widetilde{V}^0_{\text{dep}}$ (V)	$\widetilde{V}_{\text{dep}}$ (V)	$\Delta\widetilde{V}_{\text{dep}}$ (V)	$\widetilde{V}_{\text{dep}}/\widetilde{V}^0_{\text{dep}}$
LB0W0L3	184.2 ± 17.5	119.1 ± 5.6	-65.1 ± 18.4	329.5 ± 66.4	210.1 ± 16.5	-119.4 ± 67.4	0.64 ± 0.14
LB0W1L3	99.6 ± 4.3	78.3 ± 2.9	-21.3 ± 5.2	235.3 ± 24.3	179.5 ± 12.6	-55.9 ± 20.4	0.76 ± 0.07
LB0W2L3	128.2 ± 5.3	94.9 ± 4.2	-33.3 ± 6.8	270.3 ± 30.2	189.1 ± 14.2	-81.2 ± 30.9	0.70 ± 0.09
LB0W3L3	146.7 ± 13.2	109.3 ± 5.4	-37.4 ± 14.3	318.5 ± 56.1	220.7 ± 20.1	-97.8 ± 51.9	0.69 ± 0.11
LB0W0L1	127.8 ± 0.0	113.0 ± 5.9	-14.8 ± 5.9	237.3 ± 16.5	207.4 ± 16.6	-29.9 ± 13.2	0.87 ± 0.05
LB0W1L2	114.9 ± 0.0	115.2 ± 7.1	0.3 ± 7.1	190.9 ± 5.8	191.3 ± 12.4	$+0.4 \pm 10.9$	1.00 ± 0.06
LB0W2L0	119.6 ± 2.2	110.5 ± 5.6	-9.1 ± 6.0	229.6 ± 17.9	207.7 ± 18.6	-21.9 ± 15.5	0.90 ± 0.07
LB0W3L1							
LB0W4L2							
LB0W5L0	112.0 ± 7.0	106.7 ± 5.1	-5.3 ± 8.7	237.8 ± 40.7	213.3 ± 29.1	-24.5 ± 41.1	0.90 ± 0.16
LB0W4L3	125.5 ± 7.8	97.6 ± 4.1	-27.9 ± 8.8	252.5 ± 27.5	203.2 ± 13.6	-49.3 ± 22.8	0.80 ± 0.07
LB1W2L3	118.6 ± 5.0	89.0 ± 3.2	-29.6 ± 5.9	234.6 ± 37.7	170.3 ± 14.0	-64.4 ± 30.6	0.73 ± 0.09
LB1W3L3	145.8 ± 13.0	101.8 ± 5.4	-44.0 ± 14.1	295.1 ± 41.0	201.4 ± 15.6	-93.6 ± 38.9	0.68 ± 0.09
LB1W4L3	91.8 ± 4.9	71.5 ± 3.1	-20.3 ± 5.8	213.7 ± 22.6	166.9 ± 11.8	-46.8 ± 19.4	0.78 ± 0.07
LB1W5L3	113.4 ± 5.1	84.1 ± 3.7	-29.3 ± 6.3	276.8 ± 50.5	199.0 ± 21.8	-77.8 ± 50.1	0.72 ± 0.14
LB1W0L3	131.1 ± 6.3	91.7 ± 5.2	-39.4 ± 8.2	325.4 ± 55.8	186.5 ± 31.9	-138.9 ± 71.9	0.57 ± 0.16
LB1W3L1	118.9 ± 0.0	110.4 ± 5.6	-8.5 ± 5.6	306.5 ± 12.2	274.1 ± 23.2	-32.4 ± 21.6	0.89 ± 0.07
LB1W4L2	109.7 ± 0.0	100.5 ± 4.8	-9.2 ± 4.8	217.1 ± 8.3	199.7 ± 11.2	-17.4 ± 9.4	0.92 ± 0.04
LB1W5L0	119.8 ± 0.0	109.8 ± 6.6	-10.0 ± 6.6	225.8 ± 9.5	202.4 ± 16.8	-23.4 ± 15.4	0.90 ± 0.07
LB1W0L1	125.5 ± 10.9	113.4 ± 6.5	-12.1 ± 12.7	277.5 ± 40.0	242.8 ± 25.4	-34.7 ± 37.8	0.88 ± 0.12
LB1W1L2							
LB1W2L0	118.7 ± 0.0	115.7 ± 6.9	-3.0 ± 6.9	270.0 ± 22.5	260.2 ± 31.1	-9.7 ± 23.3	0.96 ± 0.09
LB1W1L3	171.7 ± 12.0	112.9 ± 6.9	-58.8 ± 13.8	322.6 ± 42.7	202.0 ± 21.3	-120.6 ± 47.5	0.63 ± 0.11

7 Evolution of Knee Voltage

As mentioned in the previous section, it would be preferable to track how the depletion voltage changes over the course of the annealing. However, doing so is impractical as it requires lowering the temperature back to that of operating operating conditions for each scan so that a reliable V_{knee}-to-$\widetilde{V}_{\text{dep}}$ can be made. Instead we rely on the V_{knee} determination to serve as a metric that characterizes the internal behavior of the silicon sensor.

For warm scans, however, the power dissipated at high voltage can create a self-heating effect that increases the current, requiring higher-order terms (i.e. $N > 1$) to be included in the polynomial in Eq. (10). This complicates the fitting procedure, so it would be desirable to find a way to account for or remove the self-heating contribution to the warm scans before the fitting is actually performed. This is discussed in Sec. 7.1.

7.1 Accounting for Self-heating

Ideally, when extracting the knee voltage from an IV curve, the sensor should be kept at a constant temperature. Self-heating combined with the limitations of our cooling system results in a non-trivial increase of the sensor temperature with bias voltage for the IV-curves measured at warm temperatures. We estimate the temperature increase of the sensor at each point in the IV scan from the power dissapated

$$\Delta T_j = T_j - 18.2 = \kappa V_j I_j \tag{3}$$

assuming a linear relationship. The constant κ was determined for each ladder with a dedicated measurement at the end of the annealing studies and 18.2 °C is the temperature assumed for unbiased sensors.

The measured current I_j is then corrected using Eq. 10 to the corresponding value $I_{corr,j}$ at $T_{warm} = 18.2$ °C. The dependence of this corrected current on the bias voltage is used to extract the knee voltage. Figure 10 shows the measured current with blue circles and the corrected current as red squares for two ladders. The triangles and open squares are from a reference measurement used to determine κ The determination of κ and consistency checks of the results are described in detail in this Appendix C.

7.2 V_{knee} Evolution

Figure 11 shows the individual fits to the warm scans taken over the course of October 2011. On the right-hand plot are the associated V_{knee} values, where the uncertainties are derived from the pseudo-experiment method described in Sec. 4.1. These plots are "raw" fits in that they do not apply the temperature corrections as described above.

The central value of the κ corrections are then applied to the warm IV scans, and the IV fits are repeated. The fits and their associated uncertainties are shown in Fig. 12. As the IV scans exhibit simpler behavior when the temperature corrections are applied, on a first-order term (i.e. $N = 1$) is required in the fit function.

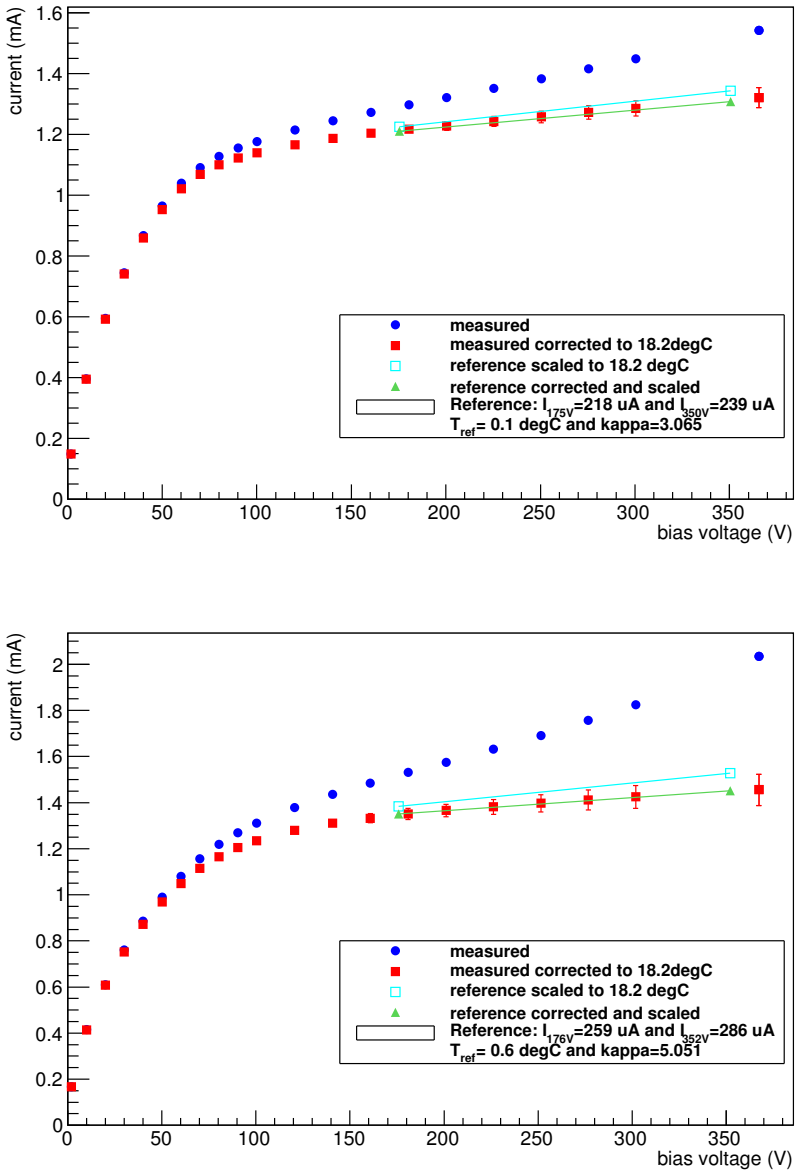

Figure 10: The measured bias current as a function of bias voltage is plotted with blue circles. The equivalent current at 18.2 °C is shown with solid red squares. The open cyan squares show the reference measurement scaled to 18.2 °C and the green triangles the reference measurement first corrected for self heating and then scaled to 18.2 °C.

A general feature of the temperature corrections is that the V_{knee} determinations are shifted to higher values when they are applied to the warm IV scans. A comparison of the V_{knee} values as determined by the raw ("Default") fits and the temperature-corrected fits is shown in Fig. 13. The "Central", "Up" and "Down" points correspond

to keeping κ at its central value, and by varying κ by plus and minus one standard deviation, respectively. We decide to quote the V_{knee} values as determined by the "Central" corrections. To include the $\pm 1\sigma_\kappa$ variation of the temperature correction, we add the following in quadrature to the baseline uncertainty of the κ-central fit:

$$\max(|V_{\text{knee}}^{\kappa+\sigma_\kappa} - V_{\text{knee}}^{\kappa}|, |V_{\text{knee}}^{\kappa-\sigma_\kappa} - V_{\text{knee}}^{\kappa}|) \ ,$$

where the baseline uncertainty is that determined from the pseudo-experiment study described in Sec. 4.1.

The resulting V_{knee} plot is shown as a function of time in Fig. 14. To extract an overall time constant that characterizes the annealing time, we fit the V_{knee} plot to the functional form $p_0 + p_1 \exp[-V_{\text{knee}}/p_2]$, where p_2 corresponds to the fitted time constant. For ladder LB0W0L3, the result is $\tau = 8.0 \pm 4.8$ days. This analysis is repeated for all eleven narrow L00 ladders. A weighted average of the time constants from the eleven L00 ladders is performed. The result is shown on Fig. 15. The average time constant obtained is $\tau_{\text{avg}} = 6.63 \pm 0.99$ days.

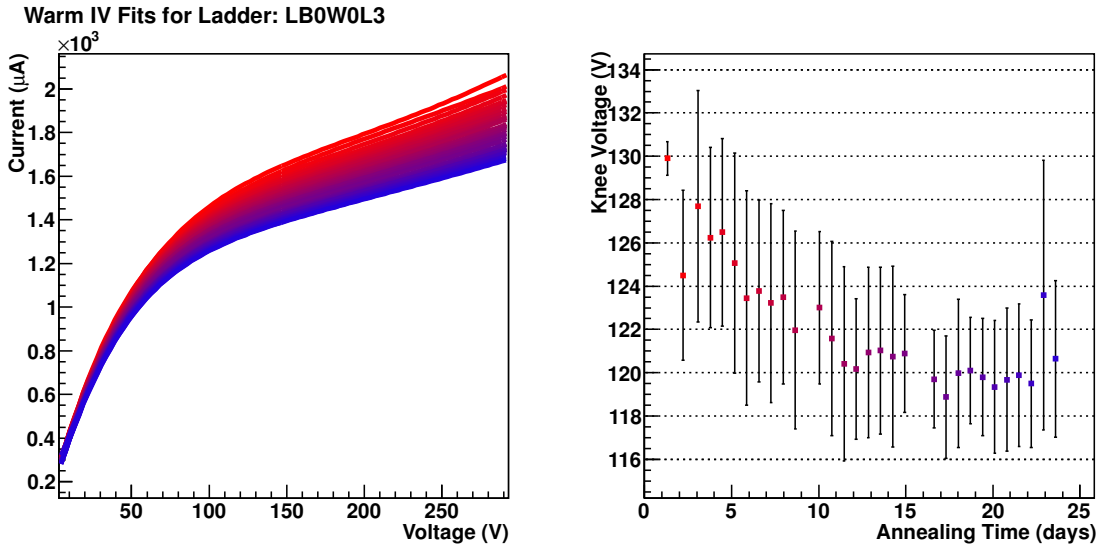

Figure 11: Raw fits and associated V_{knee} values from the warm IV scans of ladder LB0W0L3. The fits were performed with $N = 2$.

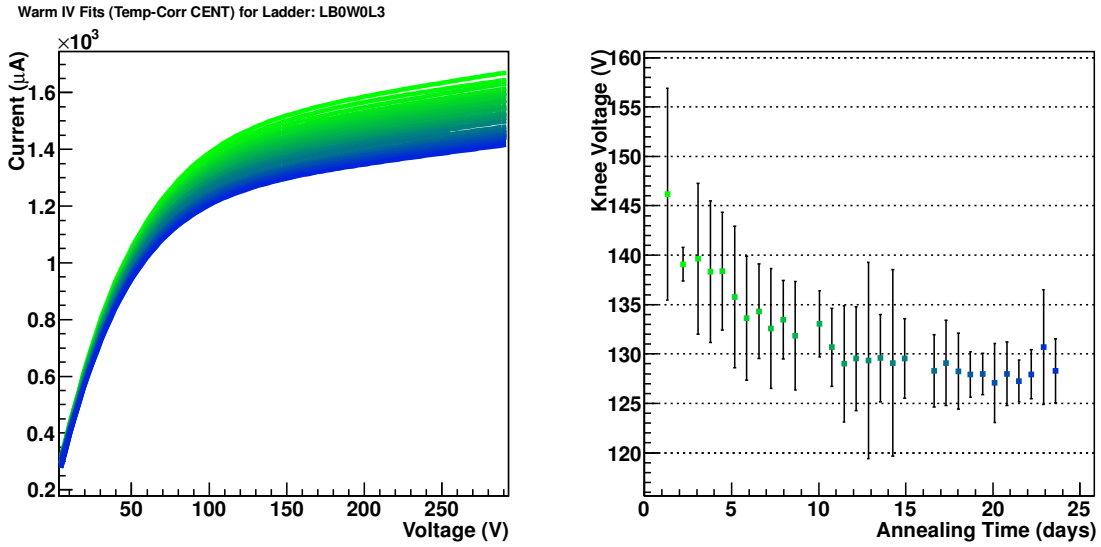

Figure 12: Fits and associated V_{knee} values from the central temperature-corrected warm IV scans of ladder LB0W0L3. The fits were performed with $N = 1$.

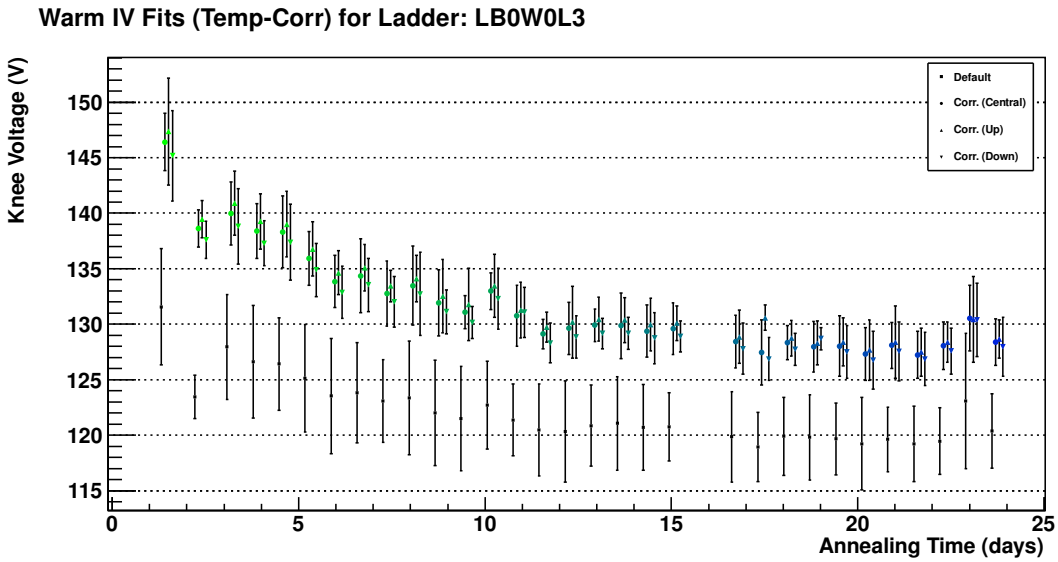

Figure 13: V_{knee} values from the raw (default) fits, and temperature-corrected fits. "Up" and "Down" correspond to varying κ by plus and minus one standard deviation, respectively.

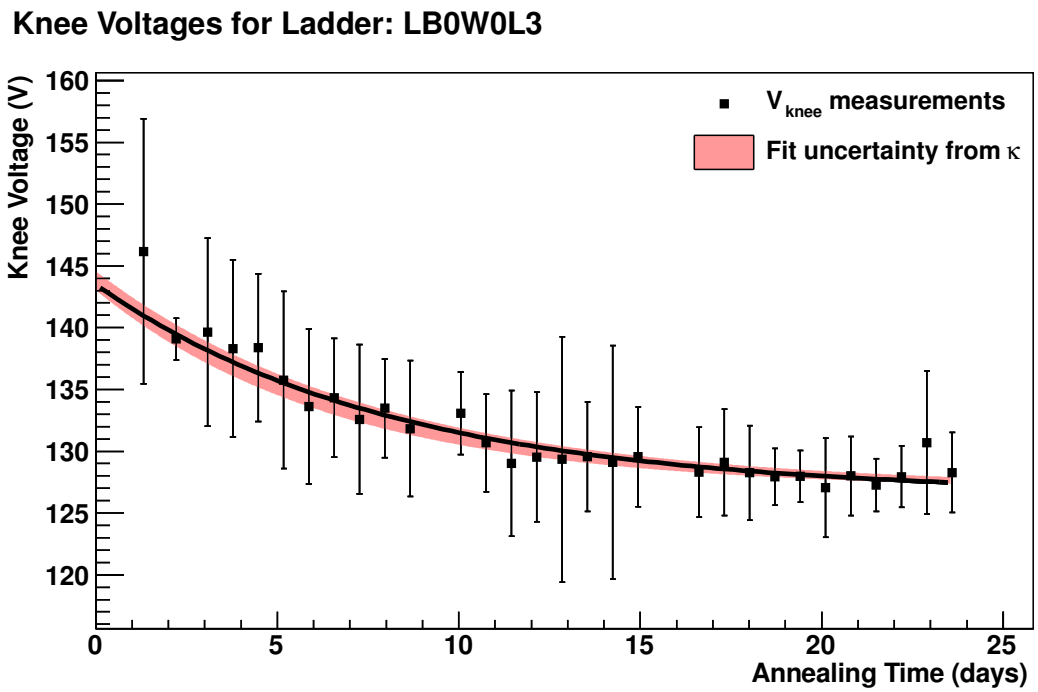

Figure 14: Exponential fit to V_{knee} values that include the systematic uncertainty from the κ values.

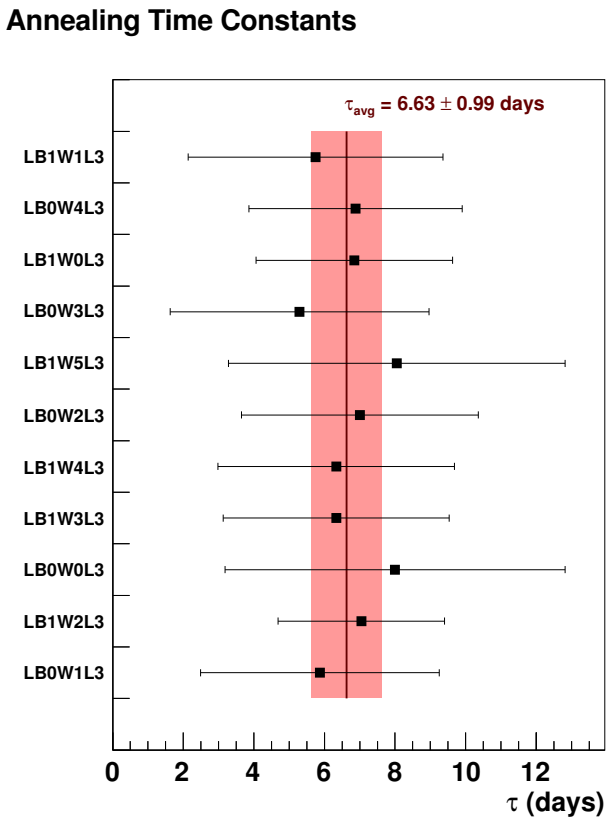

Figure 15: Annealing time constants for the eleven narrow L00 ladders, and the weighted average, assuming the measurements are uncorrelated.

8 Acknowledgments

A Analytic IV Expressions

The physical motivations for various $I(V)$ formulae are given in [1], and more comprehensively in [2, 3, 4]. We briefly summarize the case for the simple p-n junction and the more realistic case where electron-hole regeneration is included.

The expression for the current for the simple p-n junction is given by Schockley's formula:

$$I(V,T) = I_S(T)\left[\exp\left(\frac{qV}{k_BT}\right) - 1\right] \ , \tag{4}$$

where the temperature-dependence of the saturation current I_S is explicitly denoted. As the silicon detectors are operated in reverse-biased mode, the voltage V is always negative. For convenience, we define the bias voltage as $V_{\rm bias} \equiv -V$, and the bias current as $I_{\rm bias} \equiv -I$. The Schockley formula in the reverse-biased case therefore reads:

$$I_{\rm bias}(V_{\rm bias},T) = I_S(T)\left[1 - \exp\left(\frac{-qV_{\rm bias}}{k_BT}\right)\right] \ . \tag{5}$$

In reality, the additional effect of electron-hole generation is a dominant effect for low-temperature devices (no higher than 100°C). The generation term is given by

$$I_g(V_{\rm bias},T) = \frac{qn_iW}{\tau_g}\left[1 - \exp\left(-\frac{qV_{\rm bias}}{2k_BT}\right)\right] \ , \tag{6}$$

where the depletion-layer width W and generation lifetime τ_g are

$$W = \sqrt{\frac{2\epsilon_s}{qN_B}\left(V_{bi} + V_{\rm bias} - \frac{2k_BT}{q}\right)} \tag{7}$$

$$\frac{1}{\tau_g} = \frac{\sigma_p\sigma_n v_{th} N_t}{\sigma_n \exp\left(\frac{E_t - E_i}{k_BT}\right) + \sigma_p \exp\left(\frac{E_i - E_t}{k_BT}\right)} \tag{8}$$

After some significant simplications [1], the bias current $I_{\rm bias}$ can be expressed in terms of temperature T, bias voltage $V_{\rm bias}$, and other parameters (α_i) that incorporate many of the constants listed above:

$$I_{\rm bias}(V_{\rm bias},T) = \alpha_1 T^2 \exp\left(-\frac{E_g}{2k_BT}\right)\sqrt{\alpha_2\left(V_{bi} + V_{\rm bias} - \frac{2k_BT}{q}\right)}\left[1 - \exp\left(-\frac{qV_{\rm bias}}{2k_BT}\right)\right] \ , \tag{9}$$

At large values of $V_{\rm bias}$, the exponential term vanishes, and the square root argument becomes $\alpha_2 V_{\rm bias}$. One is thus able to obtain a voltage-independent expression for the

ratio of the bias currents at two different temperatures, assuming operation at large enough voltage:

$$R(T,T_0) \equiv \frac{I_{\rm bias}(V_{\rm bias},T)}{I_{\rm bias}(V_{\rm bias},T_0)} = \left(\frac{T}{T_0}\right)^2 \exp\left(-\frac{E_g}{2k_B}\frac{T_0-T}{TT_0}\right) \ . \tag{10}$$

A.1 Recommended Fit Function

Given the above discussion it might seem reasonable to assume a fit function that leads to Eq. (10). Such a suitable fit function would be:

$$I_{\rm bias}(V_{\rm bias};\mathbf{p}) = p_0\left(1-e^{-p_1 V_{\rm bias}}\right) + p_2\sqrt{p_3+V_{\rm bias}}\left(1-e^{-p_1 V_{\rm bias}/2}\right) + p_4 \ , \tag{11}$$

where the p_i represent parameters to be fitted. In principle, $p_1 = q/k_BT$ is not a parameter, but a constant. However, due to effects from experimental resolution, self-heating of the silicon sensors, and other effects that are unknown, the IV curves observed in the L00 and SVX detectors do not closely follow the behavior as given in Eq. (11). For this reason we consider a more empirical expression that gives greater flexibility in fitting the observed IV points:

$$I_{\rm bias}(V_{\rm bias};\mathbf{p}) = p_0 - p_1\exp\left(-p_2 V_{\rm bias}^{p_3}\right) + \sum_{n=1}^{N} p_{3+n} V_{\rm bias}^n, \tag{12}$$

where $1 \le N \le 3$. Whereas p_0 is left unconstrained, parameters p_1 through p_{3+N} must be positive. In addition, p_3 is constrained to be within $0.7 \le p_3 \le 1.3$. Allowing N to be other than unity gives the fit function some flexibility in accounting for self-heating effects. However, since we base our results solely on temperature-corrected IV curves (*i.e.* IV characteristics corrected for self-heating), the linear term $N = 1$ is adequate and will be the assumed context of the entire document.

B Sensor temperature estimates for various conditions

The reference measurement used to extract the value of κ for each ladder was performed after the warm period of the annealing studies. The readout chips were unpowered, the sensors unbiased, the SVX chiller setpoint at 0 °C and the ISL chiller setpoint at +6 °C. The 12 temperature sensors on the SVX bulkheads were all within the range -0.1 to 0.3 °C and randomly distributed. The 4 temperature sensors along each of the two L00 cooling lines ranged from -1.3 to 0.1 °C and were consistent with a 1 °C rise in temperature along each line, likely in response to the small flow of dry nitrogen gas through the system, necessary to avoid condensation. From this information, we estimate the average temperature of the narrow L00 sensors to be

$T_{ref} = 273.0 \pm 1.0 \pm 1.0$ K where the first term is the uncertainty on the average value and the second reflects the possible spread in temperatures among the sensors.

During the warm period of annealing studies, unbiased L00 ladders were at a temperature of 18.2 ± 0.5 °C. This is estimated from the measured temperatures of the cooling lines, ranging from 17.9-18.3 °C for both SVX and L00, without indication of any temperature gradients. The nitrogen flow was reduced for these warm settings, and the ambient sensors indicated 16-17 °C. To ensure that the ladders under study were not heated by their neighbors, the I-V scans were performed for only eight ladders at a time, each cooled by a different cooling line in the detector, while the remaining ladders were unbiased. In all, 24 L00 ladders and 72 SVX ladders were studied, rotating through the 12 groups of 8 ladders with a time of 21 hours per cycle.

After the warm period of annealing studies, two sets of IV scans were performed in addition to the reference measurement. For both sets, the voltages for all ladders were varied together instead of measuring one ladder at a time. For the *cold* IV scans, the chips were not powered and the SVX chiller was set at -5 °C. The average measured bulkhead temperature was -4.8 °C and the measured temperature along the L00 cooling lines increased from -4.4 °C to -2.1 °C following the flow. We estimate the average temperature of the unbiased sensors to be $-2.5 \pm 2.5 \pm 1.2$ °C where the first term reflects the spread in sensor temperature and the second the uncertainty on the average. The *operating* IV scans were done under normal run II operating conditions, with the chips powered and the SVX chiller set to -10 °C. The measured temperature along the L00 cooling lines increased from -8.7 °C to -3.2 °C following the flow. We estimate the average temperature of the unbiased sensors for operating conditions to be $-4.0 \pm 3.0 \pm 2.5$ °C.

C Details in Accounting for Self-heating

C.1 Determination of Power Coefficient κ for Narrow Ladders

After the warm period of the annealing studies, a dedicated measurement of the bias current of each sensor at a known temperature was performed at two values of the bias voltage: the operating voltage V_{op} and half of the operating voltage $0.5 * V_{op}$. These measurements can be scaled up $I_{refwarm}$, to equivalent current at 18.2 °C with Eq. (10). Figure 10 shows these measurements for a single ladder. The measured reference values are included in the legend and the equivalent current at 18.2 °C shown as open squares.

The blue circles are the warm IV scan measured at the end of the annealing period. The precision of the current measurement itself is 1 μA and any visible error bars reflect thermal instability of the current over the measurement period. The red squares are the equivalent current I_{corr} at a temperature of 18.2 °C, calculated with Eqs. (3) and (10). The values of κ and T_{ref} which give the best agreement between $I_{ref,warm}$(green line) and I_{corr}(solid red squares) are determined and tabulated in the legend. In the case that the bias voltage settings for the IV-scans were not exactly the same as the reference measurements, a linear extrapolation between the two reference measurements is used.

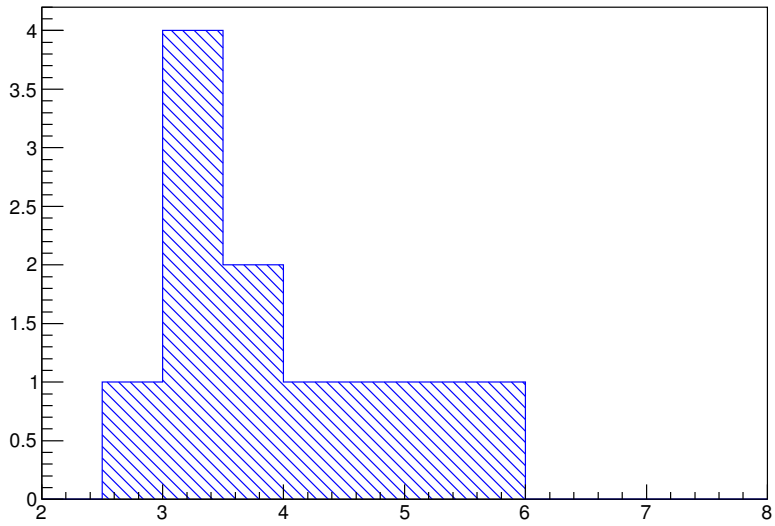

Figure 16: The distribution of κ for the 11 narrow ladders.

A second iteration is used to improve this result by accounting for any heating during the reference measurement. The value of κ found in the initial step is used to correct the currents of the reference measurements, and then the calculation of κ described above is redone with the new reference currents. All ladders converged on a stable value for κ with 3 or fewer such iterations. The final reference currents, corrected for heating and scaled to 18.2 °C, are shown with triangles in figure 10. The change in κ from the first iteration to the final one is taken as a systematic error, and is shown with error bars on the red squares in figure 10.

The best fit values of κ and T_{ref} are shown in figure 16 and 17. These values depend on the ladder location and thermal connection to the cooling lines, and may vary ladder to ladder. The best fit values of T_{ref} and κ have common systematic errors. Evaluate 0.5 °C from the uncertainty on $T_{warm} = 18.2 \pm 0.5$ °C and 1.0 °C from the uncertainty on the effective gap energy $E_{gap} = 1.21 \pm^{0}_{-0.11}$ discussed in Appendix A. They agree with the expectation $T_{ref} = 273.0 \pm 1.0 \pm 1.0$ K derived from the measured cooling line temperatures during the reference measurement, detailed in Appendix B. For κ, these two uncertainties combine to ± 0.05 K/W

The time delay between the last warm IV scan and the reference measurement is different for each ladder and varies from 3 to 24 hours. The current at fixed temperature and voltage decreases due to annealing during this time, but is observed to be less than 0.5% for the longest time period and the resulting shift in T_{ref} and κ is negligble.

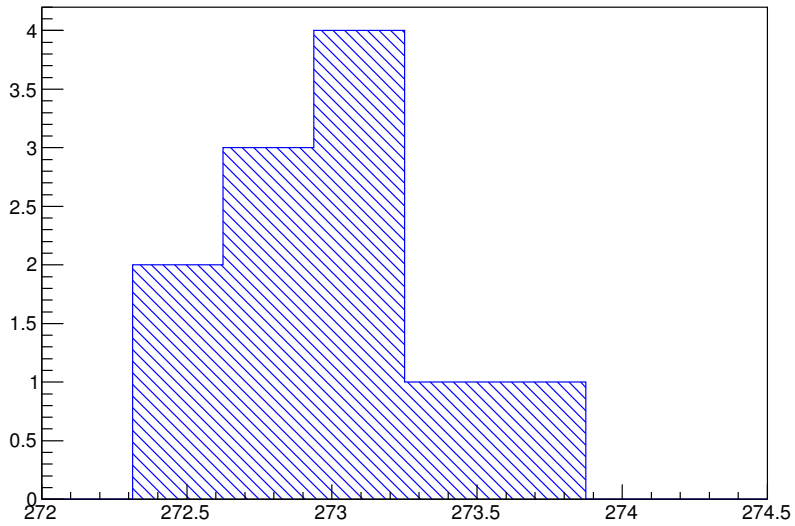

Figure 17: The distribution of T_{ref} for the 11 narrow ladders.

C.2 Wide Ladders

The results for the wide ladders look very nice except for the temperature discrepancies discussed in the next section. Figure 18 shows the measured and corrected IV scan for a typical wide ladder.

Figures 19 and 20 show the distribution of κ and T_{ref} for the wides and the narrows. While the reference temperatures are very similar, the values of κ are twice as large for the wides. κ tells how many degrees K the temperature rises when the sensor dissapates one watt of power, so the shift to larger values of κ for the wides suggests a weaker thermal connection to the cooling system.

Figure 21 shows the placement of the narrow and wide sensors (in red) on the carbon fiber support. The fraction of the surface area of the sensor that is in thermal contact with the carbon fiber is much smaller for the wide sensors, and explains the larger values of κ.

However, some of the cross checks discussed below reveal that the wides are not completely understood. In particular, there are indications that the measured values of κ are 5-10% too large. This statement is my unproven conclusion after many hours of looking at the data from IV scans, consistency checks and fits of the warm current decrease during the annealing period (not discussed in this note.) One possible explanation is the thermal instability of the warm current at the maximum voltage of the IV scan. This measured current plays a large role in the determination of κ, and if there was insufficient measurement time to reach thermal stability then the measured values woule have a systematic shift from the actual values of the currents after complete thermalization. Another explanation is that for these large quantities of dissapated power,

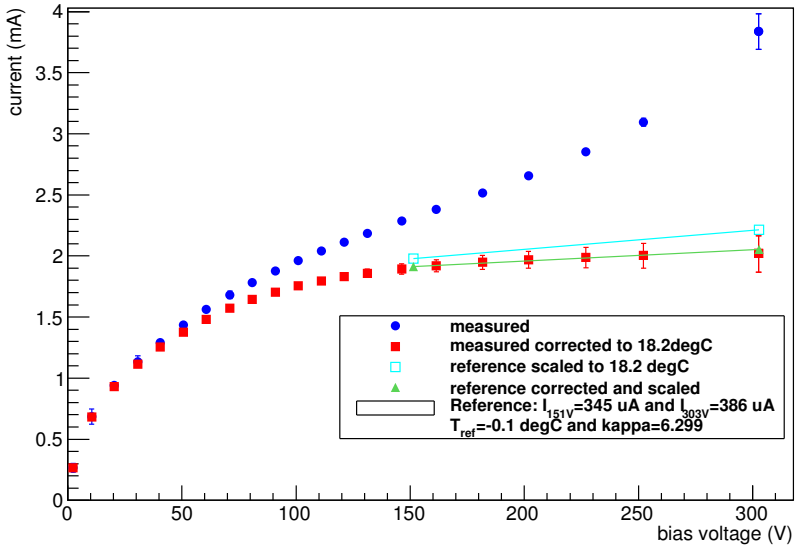

Figure 18: The measured bias current as a function of bias voltage is plotted with blue circles for a typical wide ladder. The error bars reflect the thermal stability of the measurement. The equivalent current at 18.2 °C is shown with solid red squares. The open cyan squares show the reference measurement scaled to 18.2 °C and the green triangles the reference measurement first corrected for self heating and then scaled to 18.2 °C.

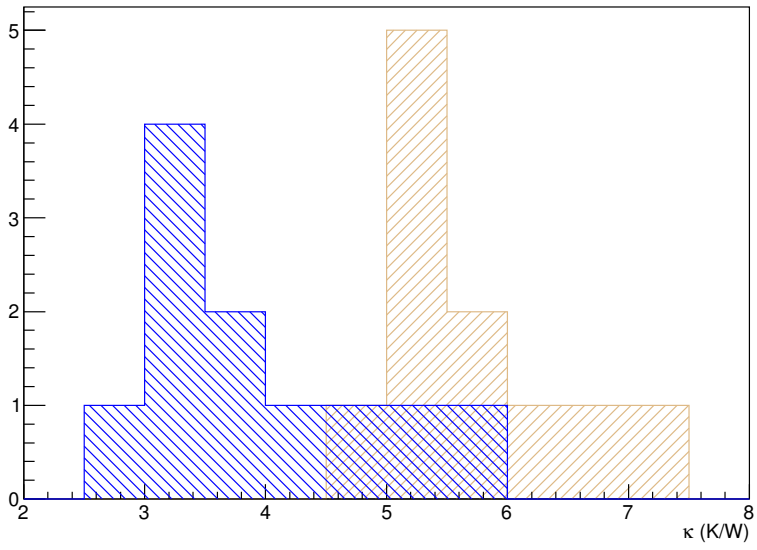

Figure 19: The distribution of κ for the 11 narrow and 11 wide ladders.

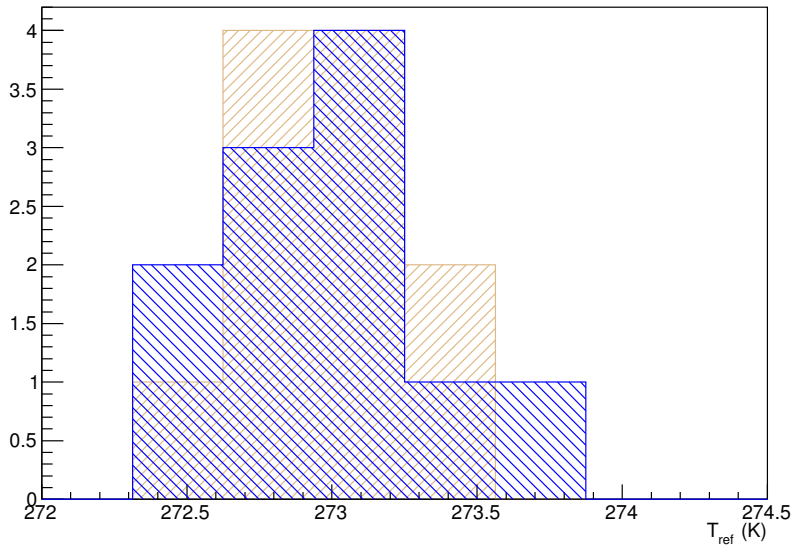

Figure 20: The distribution of T_{ref} for the 11 narrow and 11 wide ladders.

the linear relationship assumed between temperature and power is no longer valid. In either case, one could imagine disregarding the high voltage points and redoing the κ determination procedure. However, we ran out of time and motivation.

C.3 Cross checks

There were many measurements done during the annealing studies, and we can test to see if they are all internally consistent.

Consistency of currents among reference, cold and operating scans We can check the consistency among the current measurements close in temperature done after the annealing period, where systematics from E_{gap} and changes in the IV shape with temperature are small. The measurements are labelled *reference*, *cold*, and *operating* and described in Appendix B. All these measurements were done at relatively cold temperatures, so dissapative heating from a single ladder is negligible. However, all the ladders were scanned together for the cold and operating measurements, and how the heat generated by having all the ladders biased at once affects an individual ladder's IV scan is not known, and provides a large uncertainty.

The ratio of the measured currents at full bias voltage is not consistent with the measured cooling line temperatures - either the sensors are warmer than expected for the reference measurements or the sensors are cooler than expected for the cold/operating measurements. Furthermore, the disagreement is much larger for the wides than the narrows. If we assume that the sensors were at 0 °C for the reference measurement,

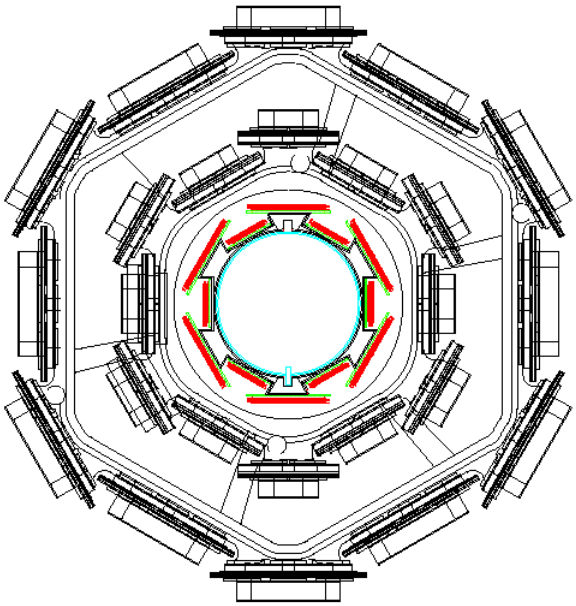

Figure 21: A diagram showing the position of the L00 sensors on the carbon fiber support structure.

then current measured at the operating (cold) scans implies that the sensor temperature was -9(-4) °C for the narrows and -12(-7) °C for the wides while the average cooling line temperature was -5(-3) °C. The average cooling line temperature for the reference measurement was -0.6 °C. For the narrows, these measurements are barely consistent within our systematic errors. However, the wides are beyond explanation - the sensors just cannot be colder than the cooling lines and the nitrogen/air.

Assuming that we correctly understand the temperatures of the sensors under the various conditions, the only explanation I can think of for this observed behavior is a constant negative offset on the measured current for 0 V. It would have to be an offset of different magnitude for the narrows and the wides, but fairly consistent among the individual sensors. I see no evidence of this in the current plotter ntuples - the current is exactly 0 whenever the voltage is below 1 V for most ladders. However, if the voltage was switched off, the current measurement might have also been switched off, or negative values reported as 0. If I play with the offset to get a reasonable temperature scaling, the shape of the cold IV curves is radically different for the narrows and the wides because the offset is -25 uA and -100 uA respectively, so this does not appear to

Figure 22: A photograph of the L00 carbon fiber support structure.

be the correct explanation. However, the effect on κ of a 25 uA offset is only 1-3% and well within the systematic error.

	cooling line temps	I_N/I_W
operating	(-8.8,-3.0) °C	0.95
cold	(-4.4,-2.0) °C	0.96
reference	(-1.2,+0.1) °C	0.65
warm corrected	18.2 °C	0.66

Table 3: At 250 V, linear extrapolation from neighboring points.

The only option I see is to blame this discrepancy on our ignorance of the thermal conditions inside the SVX tube, especially for the cold and operating measurements when all the sensors were scanned together. The systematic error on κ should cover all the possible sources of error that can affect the reference measurement. I documented all this here hoping someone would find a satisfying explanation for the inconsistency.

Expected currents from radiation dose Another cross check is to calculate the expected ratio of bias currents at fixed temperature and voltage for the narrows and the wides from the different radiation dose for the two layers, and then compare to the measured values. The current per unit volume of silicon scales linearly with radiation dose Φ, and the ratio Φ_N/Φ_w is expected to be 1.32 based on the distance from the cylindrical detector axis and the radiation field measured with TLDs. The TLD measurements were made outside ISL, so extrapolating close to the axis has an unquantified uncertainty.

The ratio of the measured current for a narrow sensor and a wide sensor, I_N/I_W, is expected to be

$$\frac{\Phi_N}{\Phi_w} = \frac{I_N/V_N}{I_W/V_w} = \frac{I_N}{I_W}\frac{V_W}{V_N} \tag{13}$$

$$\frac{I_N}{I_W} = \frac{\Phi_N}{\Phi_w}\frac{V_N}{V_W} = (1.32)(0.568) = 0.75 \tag{14}$$

and the actual measured ratios (averaged of the subset of sensors studied) are given in table 3

The reference measurements have a ratio closer to that expected from the radiation dose, suggesting that the temperature for the wides and narrows is indeed different for the cold and operating measurements.

References

[1] K. J. Knoepfel, *CDF Note 10759: Fit Functions for IV Characteristics: Silicon Annealing After Run II.* (2012).

[2] S. M. Sze, *Physics of Semiconductor Devices.* John Wiley & Sons, New York, 2nd Edition, 1981.

[3] S. M. Sze, *Semiconductor Devices: Physics and Technology.* John Wiley & Sons, New York, 1985.

[4] Kwok K. Ng, *Complete Guide to Semiconductor Devices.* John Wiley & Sons, New York, 2002.

[5] A. Chilingarov, *Generation current temperature scaling.* RD50 Technical Note, 2011

[6] Michael Moll, *Radiation Damage in Silicon Particle Detectors.* Ph. D. Dissertation, Universität Hamburg, 1999.

[7] H. Moser, *Silicon detector systems in high energy physics.* Progress in Particle and Nuclear Physics 63 (2009) 186-237.

[8] Peter Dong *et al*, *An Analysis of Bias Currents in SVX II.* CDF Note 8219, 2006.